Journal of Imaging Science and Technology® 61(4): 040408-1–040408-9, 2017.

An Adaptive Combination of Dark and Bright Channel Priors for Single Image Dehazing

Vincent Whannou de Dravo
The Norwegian Colour and Visual Computing Laboratory, NTNU, Gjøvik, Norway
E-mail: vincent.whannou.de.dravo@gmail.com

Jessica El Khoury
Le2i, FRE CNRS 2005, Université Bourgogne Franche-Comté, Dijon, France

Jean Baptiste Thomas▲
The Norwegian Colour and Visual Computing Laboratory, NTNU, Gjøvik, Norway
Le2i, FRE CNRS 2005, Université Bourgogne Franche-Comté, Dijon, France

Alamin Mansouri
Le2i, FRE CNRS 2005, Université Bourgogne Franche-Comté, Dijon, France

Jon Yngve Hardeberg▲
The Norwegian Colour and Visual Computing Laboratory, NTNU, Gjøvik, Norway

Abstract. *Dehazing methods based on prior assumptions derived from statistical image properties fail when these properties do not hold. This is most likely to happen when the scene contains large bright areas, such as snow and sky, due to the ambiguity between the airlight and the depth information. This is the case for the popular dehazing method Dark Channel Prior. In order to improve its performance, the authors propose to combine it with the recent multiscale STRESS, which serves to estimate Bright Channel Prior. Visual and quantitative evaluations show that this method outperforms Dark Channel Prior and competes with the most robust dehazing methods, since it separates bright and dark areas and therefore reduces the color cast in very bright regions.* © *2017 Society for Imaging Science and Technology.*
[DOI: 10.2352/J.ImagingSci.Technol.2017.61.4.040408]

INTRODUCTION

Haze is an atmospheric phenomenon, which leads to visibility degradation in digital images. Dehazing is a process that aims to enhance visibility and reduce the undesirable effects present in hazy images.[1–5] Dehazing is needed in several applications of computer vision, such as object recognition and tracking in bad visibility conditions.[6]

Visibility Degradation Model

In the presence of haze, the observed intensity of light coming from an object from a given point of view is the sum of two processes that occur concurrently, as shown in Figure 1. One is the direct transmission Jt, which is the light energy that emanates from the scene toward the observer. It is a fraction of the scene radiance $J(x)$, which is gradually attenuated by scattering and absorption along the line of sight. The other is the airlight A that comes from a light source (i.e., Sun), and it is redirected by the haze particles toward the observer.[7] The formation of hazy images is physically presented by the Koschmieder model[8] represented in Eq. (1). For each pixel x, the hazy image $I(x)$ formed on the camera sensor is the sum of the scene radiance $J(x)$ and the airlight $A(x) = A_\infty(1 - t(x))$, weighted by a transmission factor $t(x)$:

$$I(x) = J(x)t(x) + A_\infty(1 - t(x)). \tag{1}$$

The atmospheric light A_∞ is the airlight scattered by the fog when the object is at infinite distance from the observer. The transmission factor $t(x)$ depends on the scene depth d (distance from the sensor) and the scattering coefficient β of the haze, such that $t(x) = e^{-\beta d(x)}$ and $t \in [0; 1]$. The transmission factor t tends toward zero when it accounts for distant objects or heavy haze and is close to 1 when it accounts for near objects or light haze. Unlike other traditional image degradations, haze/fog has some degrading particularities. It is a natural, depth-dependent perturbation that spans non-uniformly over the whole image. The degradation and the loss of information increase with depth, as the amount of fog between the imaged surface and the sensor increases. Hazy and foggy images also have different prevailing colors, which depend on the density of the scattering particles and the ambient light. The process to recover $J(x)$ from $I(x)$ is known as dehazing or defogging.

▲ IS&T Members.

Received Feb. 28, 2017; accepted for publication June 21, 2017; published online July 24, 2017. Associate Editor: Yeong-Ho Ha.
1062-3701/2017/61(4)/040408/9/$25.00

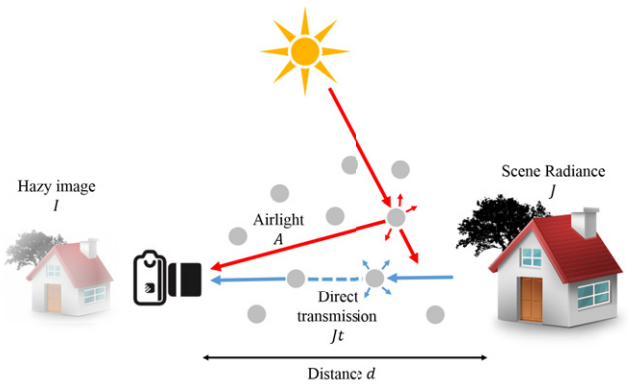

Figure 1. Imaging through haze. The observed intensity of light I coming from an object placed at distance d from the camera is controlled by two processes. One is the direct transmission Jt, which is the light energy that emanates from the scene toward the observer. It is a fraction of the scene radiance J, which is gradually attenuated by scattering and absorption along the line of sight. The other is the airlight A, which comes from a light source (i.e., Sun) and is scattered by the haze particles toward the observer.

State of the Art of Dehazing Methods

Two main categories of dehazing approach are usually considered. The first relies on inversion of the physical model of haze Eq. (1). The second aims to enhance the quality of the image according to the visual experience without considering Koschmieder's model. Both approaches provide good performance on natural scenes of homogeneous light haze.[9] However, they both fail when it comes to enhancing the visibility of scenes that contain white objects, snow or heavy haze. Methods that estimate the Koschmieder model parameters do not provide particularly good results when there are too many white objects in the scene, as the haze density is estimated over the dark pixels. They also fail when removing a heavy haze or the haze over distant objects, where the related physical model is almost invalid.[10] Although image enhancement algorithms meet real requirements, they also fail in the aforementioned situations. Some examples of these failures are shown in Refs. 11–13.

We separate the first category into two subcategories. The first one consists of using some additional information besides the color hazy image that can help to break down the ill-posedness of the problem. For instance, Narasimhan et al.[4] and Schechner et al.[5] indicated how to take advantage of two images of the same scene taken under different weather conditions or with different polarizer orientations, respectively. Kopf et al.[14] associated the corresponding depth map with the hazy image. In Refs. 15, 16, dehazing is performed based on the dissimilarities between the RGB and the near-infrared image of the same scene. Methods belonging to the second subcategory consider only the hazy image. They are mainly based on prior assumptions deduced from a large collection of similar images. For instance, Fattal[17] made his estimation based on independent component analysis. He et al.[11] proposed a solution based on the Dark Channel Prior (DCP) assumption explained below. Tarel and Hautière[18] proposed a dehazing method based on a filtering approach. Their method consists of estimating the atmospheric light as the median of the minimal channel of the image and deducing the transmission parameter of the Koschmieder model (1) through a bilateral filter, which has good behavior at the edges and the corners. Local smoothing is applied to reduce noise and artifacts.

The second category includes the methods that combine image enhancement tools with the properties of the haze physical model. Based on the assumption that a dehazed image has a higher contrast than its corresponding hazy image, Tan[19] proposed an optimization based on Markov random field. Galdran et al.[20,21] assumed that the physical model is too simple to model the real situation, and fails to handle change of size of the atmospheric particles and the spatial non-uniformity of the illuminant. Thus, they developed a variational framework for contrast enhancement of hazy images that considers spatially variant features. Recently, Whannou de Dravo and Hardeberg[22] proposed a multiscale version of STRESS (M-STRESS) for dehazing. Based on the STRESS framework,[23] they combine edge detection and the Hidden Markov Model (HMM). In M-STRESS, they use a spatial algorithm STRESS (Spatiotemporal Retinex-inspired Envelope with Stochastic Sampling) to approximate the haze model. Through the STRESS framework, which is a simplification of the Retinex algorithm or the ACE algorithm,[24] the reflectance of the scene is estimated based on the concept of two envelopes, the minimum and maximum envelopes calculated on a circular patch centered at a given pixel within the image. More details are given in the M-STRESS section.

Observation and Contribution

According to He et al.,[11] the DCP hypothesis is stated as follows: *in most of the non-sky patches of natural color scenes, at least one color channel has some pixels whose intensity values are very low and close to zero*. This statistical observation defines the dark channel, from which the transmission factor t and the atmospheric light A_∞ are estimated (refer to the DCP section).

From the DCP hypothesis, we deduce the Bright Channel Prior (BCP) assumption, which states that *for sky and bright areas, every color channel in the haze-free image has a pixel with a high intensity, which is close to 255 if we consider an image with 8 bits per channel.*[22] The BCP is approximated by the maximum envelope of the image, which is calculated and enhanced through the M-STRESS method. Several dehazing algorithms are based on the DCP hypothesis.[18,19,22,25] They usually suffer from some drawbacks: since this hypothesis depends on the dark pixels in the scene, the DCP fails to estimate the transmission when the light coming from an object is similar to the atmospheric light. Thus, DCP based methods are not good at restoring images with a large bright area such as snow or sky. Since it has been proved in Ref. 13 that a good labeling of pixels should overcome the color cast in bright regions, our first goal in this article is to verify whether the BCP holds in bright regions as the DCP holds already in dark regions. The second goal consists of unifying both concepts into

the same framework. Thus, we combine the DCP method[11] and M-STRESS.[22] The BCP cannot be directly derived from the DCP (cf. the Proposed Method section) since it does not simplify the ill-posedness of the haze model. Thus, the BCP is estimated thanks to the maximum of the STRESS algorithm from two scales (cf. the M-STRESS section). This combination provides a beneficial enhancement of the overall quality, observed through visual and objective assessment. Since the processing of bright and dark areas is performed separately, the color cast is remarkably reduced in very bright regions.

In the following sections, we introduce the dehazing steps of both the DCP and M-STRESS methods. We then describe how these methods are applied on segmented parts of the same image, which represents one of the scenarios that causes failure of previous methods. Finally, we discuss the results and further ways to overcome limitations.

THE DCP

Dark Channel Estimation

Based on the DCP hypothesis stated earlier, the dark channel J^{dark} is the minimum intensity value over the channels, red (r), green (g) and blue (b), of a local patch $\Omega(x)$ centered on each pixel x within the image. It is formally defined as follows:

$$J^{\text{dark}}(x) = \min_{c\in\{r,g,b\}} \left(\min_{y\in\Omega(x)} (J^c(y)) \right), \tag{2}$$

where J is the scene radiance, as in Eq. (1). The low intensities within the dark channel are usually due to shadows and dark or colorful surfaces. The dark channels J^{dark} are usually computed using a patch size of 15×15. The definition of the patch size is critical. A large patch increases the probability that a patch contains dark pixels. Therefore, the dark channel can be accurately estimated. However, with a large patch, the assumption that the transmission is constant within a patch becomes less appropriate and the halo artifacts near depth edges in the dehazed image become stronger.[11]

Atmospheric Light Estimation

As the dark channel of a hazy image is supposed to approximate the haze density well, it is used to estimate the atmospheric light. The atmospheric light A_∞ is estimated by picking 0.1% of the brightest pixels in the dark channel. Among these pixels, the pixel with the highest intensity in the input image is selected as the atmospheric light.[11]

Transmission Estimation

The transmission t is estimated from the airlight as follows:

$$t(x) = 1 - w \min_c \left(\min_{y\in\Omega(x)} \left(\frac{I^c(y)}{A^c_\infty} \right) \right) \tag{3}$$

$$= 1 - 0.95X, \tag{4}$$

where $X = \min_c(\min_{y\in\Omega(x)} (I^c(y)/A^c_\infty))$. Here, w is the amount of haze kept in the image to avoid unnatural scenes. It is fixed to 0.95 in Ref. 11. In Eq. (3), t behaves as the complementary in [0, 1] of the hazy image. Due to the halos that this estimation can induce in the output image, the transmission is refined by making an analogy between the haze model and the matting equation.

Scene Radiance Recovery

After estimating the unknown parameters A_∞ and t of Eq. (1), the haze-free image is calculated as follows:

$$J(x) = \frac{I(x) - A_\infty}{\max(t(x), t_0)} + A_\infty. \tag{5}$$

The scene radiance is usually not as bright as the atmospheric light, so the image looks dim after dehazing. To avoid dim images or a division by zero, t_0 is set equal to a typical value of 0.1.

THE M-STRESS METHOD

The STRESS framework introduced in Ref. 23 for contrast enhancement and color correction was adjusted in Ref. 22 to be applied to the dehazing problem. According to the observation that a relatively bright detail in a very bright region of an image appears darker than a darker detail in a very dark region, Kolås et al.[23] calculated, for each pixel within the image, local reference lightness and darkness points for each color channel. Thus, for each pixel in a circular patch, a maximum and a minimum envelope are calculated in an iterative manner.

They represent the envelopes that contain the image signal. The calculation of these envelopes and their relationship with the haze model formulation is provided in the following paragraph.

For each pixel $I^c(x)$ in each color channel c, M pixels are sampled according to a random sampling with probability proportional to the Euclidean distance in the image from the sample pixel $I^c_j(x)$ $(\neq I^c(x))$, $j \in \{1, \ldots, M\}$, to the pixel $I^c(x)$. These pixels are randomly sampled i times from a circular patch with radius *rad* centered at $I^c(x)$. For one iteration i, where $i \in \{1, \ldots, N\}$, the maximum and the minimum samples are calculated as follows:

$$I_i^{\max,c}(x) = \max_{j\in\{1,\ldots,M\}} I^c_j; \quad I_i^{\min,c}(x) = \min_{j\in\{1,\ldots,M\}} I^c_j. \tag{6}$$

As $I^c(x)$ is included in the sampled set, $I_i^{\min,c}(x) \le I^c(x) \le I_i^{\max,c}(x)$.

The range r^c_i of the sampled pixels and its normalized value $v^c_i \in [0, 1]$ are given as

$$r^c_i(x) = I_i^{\max,c}(x) - I_i^{\min,c}(x); \tag{7}$$

$$v^c_i(x) = \begin{cases} 1/2, & \text{if } r^c_i = 0, \\ ((I^c(x) - I_i^{\min,c}(x)))/r^c_i(x), & \text{else.} \end{cases} \tag{8}$$

These parameters are averaged over the N iterations in order to refine estimation:

$$\bar{r}^c(x) = \frac{1}{N}\sum_{i=1}^{N} r^c_i(x); \quad \bar{v}^c(x) = \frac{1}{N}\sum_{i=1}^{N} v^c_i(x). \tag{9}$$

The maximum and minimum envelopes at each channel c, $E^{\max,c}(x)$ and $E^{\min,c}(x)$, are calculated from $\bar{r}^c(x)$ and $\bar{v}^c(x)$:

$$E^{\min,c}(x) = I^c(x) - \bar{v}^c(x)\bar{r}^c(x); \tag{10}$$

$$E^{\max,c}(x) = I^c(x) + (1-\bar{v}^c(x))\bar{r}^c(x) = E^{\min,c}(x) + \bar{r}^c(x). \tag{11}$$

As $v_i^c(x) \in [0,1]$, also $\bar{v}^c(x) \in [0,1]$. This implies that $E^{\min,c}(x) \leq I^c(x) \leq E^{\max,c}(x)$.

Local contrast enhancement of grayscale images is one of the applications of the STRESS method.[23] Thus, to obtain a local effect, the corrected value of a given pixel $I^c(x)$ is scaled between $E^{\min,c}(x)$ and $E^{\max,c}(x)$ values:

$$p^c_{\text{STRESS}}(x) = \frac{I^c(x) - E^{\min,c}(x)}{E^{\max,c}(x) - E^{\min,c}(x)}. \tag{12}$$

Considering the definitions of $E^{\min,c}(x)$ and $E^{\max,c}(x)$ in Eqs. (10) and (11), we can deduce

$$I^c(x) = E^{\max,c}(x) - (1-\bar{v}^c(x))\bar{r}^c(x); \tag{13}$$

$$I^c(x) = E^{\min,c}(x) + \bar{r}^c(x) - (1-\bar{v}^c(x))\bar{r}^c(x);$$

$$I^c(x) = E^{\min,c}(x) + [1-(1-\bar{v}^c(x))]\bar{r}^c(x). \tag{14}$$

Assuming $\bar{w}^c(x) = 1 - \bar{v}^c(x)$, as $\bar{v}^c(x) \in [0,1]$, also $\bar{w}^c(x) \in [0,1]$, and Eq. (14) becomes

$$I^c(x) = E^{\min,c}(x) + (1-\bar{w}^c(x))\bar{r}^c(x). \tag{15}$$

In order to meet the haze model in Eq. (1), we assume that $\bar{w}_1^c(x) = 1$ and $\bar{w}_2^c(x) = \bar{w}^c(x)$. Thus, Eq. (15) becomes

$$I^c(x) = E^{\min,c}(x)\bar{w}_1^c(x) + (1-\bar{w}_2^c(x))\bar{r}^c(x). \tag{16}$$

The output of the STRESS framework is given in Eq. (12). Thus, p^c_{STRESS} corresponds exactly to calculating the relative position of a pixel x of the input hazy image I within the envelopes. In other words, it stretches the contrast at pixel x:

$$I^c(x) = p^c_{\text{STRESS}}(x)\bar{w}_1^c(x) + (1-\bar{w}_2^c(x))\bar{r}^c(x). \tag{17}$$

From the above relationships, we point out some deductions and indications.

- $I^c(x)$ is the input pixel value.
- p^c_{STRESS} is the output pixel value stretched toward either $E^{\max,c}(x)$ or $E^{\min,c}(x)$.
- The minimum envelope $E^{\min}$ is equivalent to the dark channel since it can be assimilated to the local reference darkness points in each chromatic channel.[22,23]
- DCP uses a fixed single scale as a parameter to dehaze a hazy image, and all pixels in a given patch are used for estimating parameters. According to Ref. 11, the chromatic distortions change with the patch size. These effects decrease within the sky region when the patch size increases. To deal with this issue, two scales are used in M-STRESS. Each parameter in Eq. (18) is estimated according to the current pixel through a random process using some predefined number of samples in a circular patch. By doing this, the scale in this model influences all of the parameters. The atmospheric light, for instance, is computed in the first model as a constant or a scalar value in each channel without taking into account whether or not the pixel belongs to a sky region, whereas, in the second model, the estimation of this parameter takes into account the three different regions of the model: far objects, which denote objects that have dark pixels in non-dense fog; near objects, which denote objects that have dark pixels in heavy haze; and regions similar to the sky, which have bright pixels. Far objects are well enhanced using Ω_1 from STRESS, and near objects are well enhanced with Ω_2 from STRESS. The terms Ω_1 and Ω_2 are, respectively, two circular patches of radius such that

$$\text{rad}_1 = \frac{1}{10}\max(\text{width}, \text{height}),$$

$$\text{rad}_2 = \max(\text{width}, \text{height}),$$

  where width and height represent the width and height of the image.
- Comparing with (1), instead of a single transmission factor t, two parameters $\bar{w}_1^c$ and $\bar{w}_2^c$ are defined. A good simulation of t should be such that $t \epsilon [0,1]$. This is true for $\bar{w}_1^c$ and $\bar{w}_2^c$. Since $\bar{w}_1^c$ is equal to 1, it accounts only for near objects. In the case of rad_1 when the circular patch is small, $I_i^{\max,c}$ and $I_i^{\min,c}$ are close to each other. Thus, $r_i^c = I_i^{\max,c} - I_i^{\min,c}$ is small and roughly less than $1/2$ since we consider a small patch and far objects. This small value makes v_i^c a little high. As $\bar{w}_2^c$ is the complementary of v_i^c, it will be small and will therefore denote the distant objects. When the circular patch of radius rad_2 accounts for the whole image, r_i^c should be high as more pixels of different objects are considered; thus, $I_i^{\max,c}$ has the chance to be very high and $I_i^{\min,c}$ to be very low. Accordingly, v_i^c is less than $1/2$ and $\bar{w}_2^c$ is therefore high. Thus, it accounts for near objects and light haze.
- In DCP, the transmission is related to the depth. The pseudo-transmission parameter in M-STRESS is calculated separately on color channels. Therefore, even this function may have the same behavior as that defined in Eq. (1); it does not necessarily have here a physical meaning that is related to the depth.
- The other difference between the dark channel J^{dark} and the minimum envelope $E^{\min,c}$ in the way that they have been used for dehazing is the fact that the first has been applied to at least one channel while the second has been applied to all channels.

Bright Channel Estimation

From the definition given in Ref. 22, the BCP can be written formally as follows:

$$J^{\text{bright},c}(x) = \max_{\Omega^c(x) \in S}(E^{\max,c}(\Omega^c(x))) \tag{18}$$

$$\approx \max_{\Omega^c(x)\in S}\left(p^c_{\text{STRESS}}(\Omega^c(x))\right) \tag{19}$$

$$\approx \max_{\Omega^c(x)\in S}\left(J^c(\Omega^c(x))\right). \tag{20}$$

The term Ω in M-STRESS represents a given scale from the set of scales $S = \{\Omega_1(x), \Omega_2(x)\}$. In Eq. (19), $E^{\max,c}$ (from Eq. (18)) is approximated by p^c_{STRESS} and then by J in Eq. (20) to make a link with Eq. (1).

Atmospheric Light Estimation

The parameter $\bar{r}^c$ is a good approximation of the atmospheric light when the circular patch accounts for the whole image (radius rad_2). The large value of r_i^c meets the definition of the atmospheric light. It represents the haze veil that is added to the haze-free image, represented as minimum intensities for each color channel. The averaged value $\bar{r}^c$ calculated over N iterations provides a more accurate estimation. In M-STRESS, $\bar{r}^c$ is calculated for each color channel c. According to Eq. (9), the total number of iterations N has been set between 100 and 150. This value changes only in the case of STRESS and is fixed for DCP.

Transmission Estimation

In M-STRESS, two pseudo-transmissions are used. The first one, $\bar{w}_1$, is well suited for near objects since its value has been set to 1. The second one is defined as $\bar{w}_2 = 1 - p_{\text{STRESS}}$. Here, the optimization of the pseudo-transmission $\bar{w}_2$ is performed in a stochastic and iterative form. Thus, it seems clear that the transmissions in the two models are close to each other, since they can be seen as the complementary of the dark channel from the input image in the first model[11] and the complementary of the minimum envelope in the second model.[22]

Scene Radiance Recovery

The M-STRESS method estimates the haze-free image by working on either the minimum or the maximum envelope. When the calculation of the haze-free image is made using the minimum envelope, this means that the input pixel belongs to the near region or the far region. When it is made considering the maximum envelope, this implies that the algorithm is dealing with pixels in the sky region.

PROPOSED METHOD

Our method consists of segmenting an image into two parts. The dark region where the DCP holds and the bright region which is subject to BCP. Here, we assume that the image has been segmented perfectly. The algorithm DCP[11] is applied on dark regions and the algorithm M-STRESS[22] is applied on regions similar to the sky. It is worth noting here that it is more efficient to implement the BCP from the STRESS framework than from the DCP. To show this, let us take a look at the definition of the BCP directly derived from the definition of the DCP given by Ref. 11. The bright channel $J^{\text{bright},c}$ at each color channel c is calculated as follows:

$$J^{\text{bright},c}(x) = \max_{c\in\{r,g,b\}}\left(\max_{y\in\Omega(x)}\left(J^c(y)\right)\right). \tag{21}$$

According to the DCP definition, $J^{bright,c}$ has the following behavior:

$$J^{\text{bright},c}(x) \to 1. \tag{22}$$

Let us now include this in the initial equation of Koschmieder's law, Eq. (1). Following then the same steps as in Ref. 11, we have the following equation after dividing Eq. (1) by a known A^c_∞ and also applying the bright channel definition to Eq. (21):

$$\max_{y\in\Omega(x)}\left(\max_c \frac{I^c(x)}{A^c_\infty}\right) = t^c(x)\max_{y\in\Omega(x)}\left(\max_c \frac{\mathrm{J}^c(x)}{A^c_\infty}\right) + 1 - t^c(x). \tag{23}$$

Assuming that the pixel is from a bright region and taking into account the relation in Eq. (22), we have the following formula:

$$\max_{y\in\Omega(x)}\left(\max_c \frac{I^c(x)}{A^c_\infty}\right) = t^c(x) + 1 - t^c(x) = 1. \tag{24}$$

Unfortunately, from Eq. (24), we could not deduce the expression for t. Likewise, the definition of the bright channel in Eq. (21) is not formally true; thus, it does not really help to simplify the ill-posedness of the haze model. Due to the difficulty of implementing the BCP from the DCP, it is worth noting that the BCP, unlike the DCP, is not an observation deduced from natural color scenes. It may be seen as a direct consequence of the definition of the DCP. Thus, the formal definition of the BCP is as follows:

$$\forall c \in \{r, g, b\}, J^{\text{bright},c}(x) = \max_{y\in\Omega(x)}\left(J^c(y)\right) \approx 1. \tag{25}$$

Our method flowchart in Figure 2 shows the key steps to verify the validity of the DCP and BCP in different contexts. When the bright region is very large compared with the dark region, such as in snowy scenes (Figure 3), the BCP is then applied to the whole image without prior segmentation. When the sky is the main brightest part of the image, a prior segmentation is required to label bright and dark pixels, which will be dehazed by the BCP and DCP, respectively.

EXPERIMENTS

Setup

Our experiments consist of evaluating dehazing methods with hazy images that contain either sky (Figure 4) or snow and sky (Fig. 3). For this, we used the DCP algorithm and our proposed method to investigate the enhancement that the combination approach induces in comparison to DCP. We also used Tarel's method to make clear that such problems are common for methods based on the physical model of haze. For these experiments, we used the following settings.

- Considering the large dimensions of the images (4290 × 2856) we took in Gjøvik, Lake Mjøsa at the beginning of winter 2014–2015 (Fig. 3), all of these images have been resized to 1128 × 635 in order to reduce the cost in terms of calculation time.

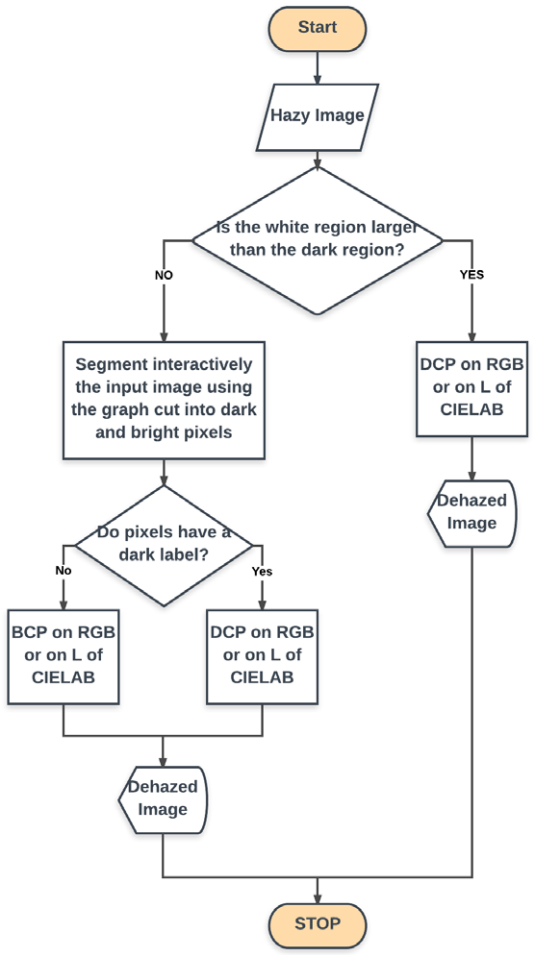

Figure 2. Flowchart of the adaptive combination of DCP and BCP for sky and snow image dehazing.

- For the algorithm developed in Ref. 11, we used the same patch size of 15 × 15 as in the original article for all of the images.
- For results obtained from Ref. 18, the default parameters introduced in the original article were used.
- For the proposed approach, settings that have been used in Refs. 11 and 12 have been combined.

To evaluate the performance of dehazing methods, dehazed images are usually assessed visually and quantitatively using blind measures.[26] This is done because of the lack of haze-free images of outdoor scenes. We uphold the visual judgment by some dehazing-dedicated metrics. *FADE* (Fog Aware Density Evaluator),[27] which is a prediction model for perceptual fog density, denotes the amount of haze remaining on the image after dehazing. This is performed through similarity computation between dehazed images, Natural Scene Statistics and fog aware statistical features. These features include those that are directly altered by haze, such as sharpness, contrast, image entropy, saturation and colorfulness. The Contrast ascension–Structural similarity metric (*CS*)[28] combines the ascension of contrast degree with the structural similarity between the hazy and dehazed images. A high structure similarity underlines a consistency of edges before and after dehazing. This means that no artificial edges such as blocking artifacts have been introduced after dehazing. Unlike *CS*, the Contrast–Naturalness–Colorfulness (*CNC*) evaluating metric[29] estimates the perceived quality of the color reproductions in terms of naturalness and saturation in addition to the contrast. A good reconstruction is denoted by *FADE* scores close to zero and high scores of *CNC* and *CS*.

RESULTS

Considering the dehazed images shown in Fig. 3, it is easy to observe that DCP based methods fail to recover natural colors of bright areas, especially in the upper part of the image. The DCP method works better on snow than on sky, since the contrast enhancement resulting from dehazing generates more unnatural colors in patches with higher saturation and they are hardly distinguishable because of the large scene depth and the high density of haze. This is seen in all images of Fig. 3 and the first two images of Fig. 4. This confirms the robustness of the DCP statement, which underlines the non-sky regions, where at least a small patch is dark. The BCP applied to the luminance channel of CIELAB in bright regions turns out to be more appropriate than the DCP. Although the DCP fails in such contexts, it performs well on the last two images of Fig. 4, where a very light haze prevails over a clear sky. We can also single out the resulting dark contrast in dark regions, which is shown clearly in the images of the second and fourth columns of Fig. 4. This results from an overestimation of the haze level. A possible relief consists of adjusting the w and t_0 parameters in Eqs. (3) and (5) to reduce unnatural and dim images.

Compared with DCP, Tarel's method produces similar color effects such as color cast, not only on the sky part, but also on the snow. These effects are more accentuated on the sky. Halo artifacts are significant near the edges separating the upper and lower parts of images. In Figs. 3 and 4, the images subject to Tarel's method remain hazy. This was stated before in Ref. 30. This is positively rated for images with light haze and foreground areas where this method keeps a natural perception of the dehazed scene. The scores presented in Tables I and II are calculated on images presented in Figs. 3 and 4, respectively. Besides the dehazed images, the scores of the no-reference metric *FADE* are calculated on the original hazy images, which contain a higher density of fog than the dehazed images. The proposed method seems to be the most efficient at fog removal for all images. According to the *CS* values, our method outperforms its peers on contrast enhancement and maintaining image structure. When color and naturalness are considered through *CNC*, it is revealed that DCP followed by Tarel's method provide a slightly better natural enhancement for light haze (the last two images of Fig. 4), as stated before from visual judgment. However, for the other images with more complicated contexts, our method has particularly better performance.

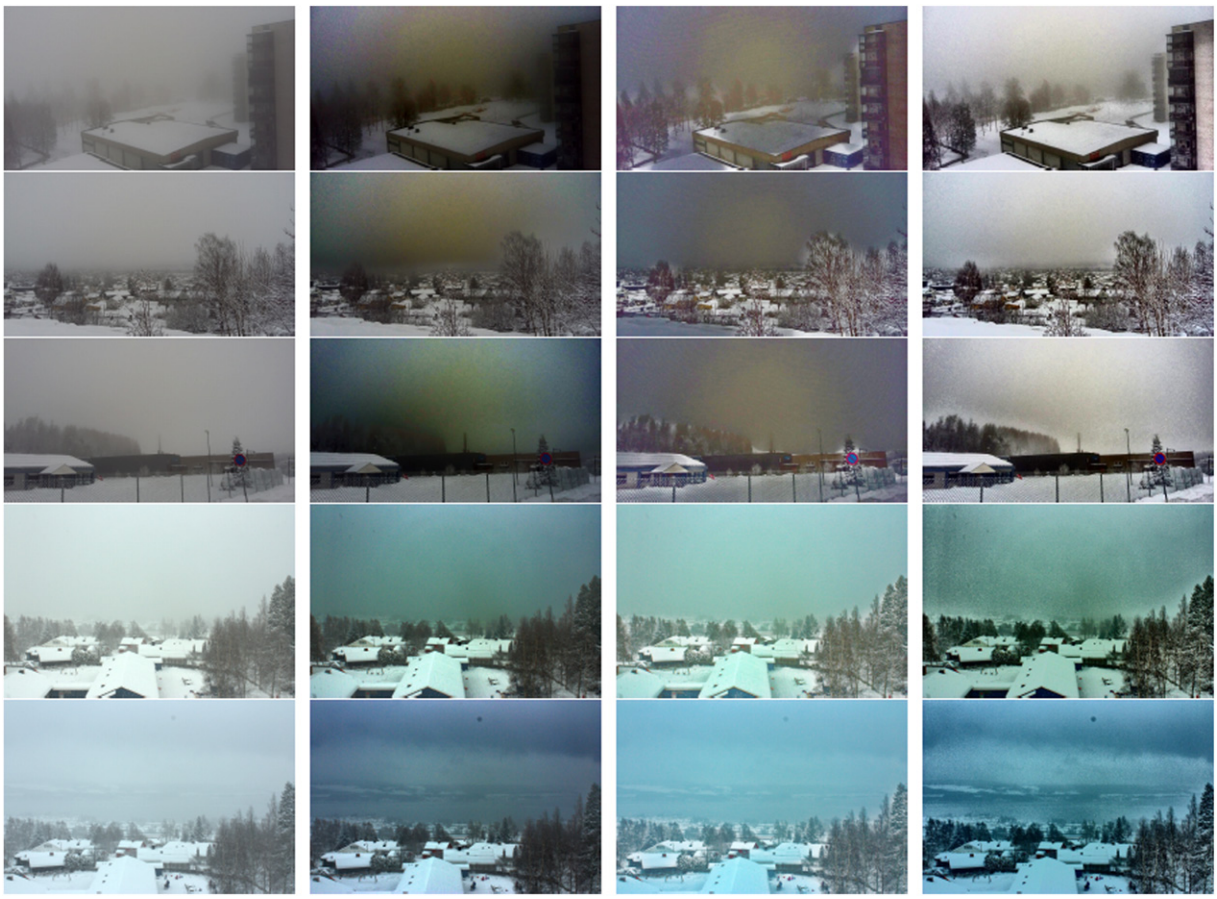

(a) (b) (c) (d)

Figure 3. From top to bottom, the images correspond to SNOW 1, SNOW 2, SNOW 3 and SNOW 4, respectively. (a) Original image, (b) He's method (DCP), (c) Tarel's method, (d) our method. We can see that DCP methods like that of Tarel are not suited for snowy hazy images.

Table I. The scores of the *FADE*, *CNC* and *CS* metrics corresponding to the images dehazed by He's method, Tarel's method and our method and presented in Fig. 3. The best scores of *FADE*, *CNC* and *CS* are given in brackets, bold and underlined, respectively. A good reconstruction is denoted by *FADE* scores close to zero and high scores of *CNC* and *CS*.

	Original image	He's method			Tarel's method			Our method		
	FADE	*FADE*	*CNC*	*CS*	*FADE*	*CNC*	*CS*	*FADE*	*CNC*	*CS*
SNOW 1	3.7868	0.7827	2.2755	0.9693	1.0293	1.5668	0.8488	(0.5019)	**2.4445**	1.6505
SNOW 2	1.3346	0.5906	1.6929	0.2959	0.5302	1.2959	0.3584	(0.3033)	**1.7583**	0.8802
SNOW 3	1.3346	0.7013	1.8090	0.9341	0.8389	1.6329	0.5710	(0.4218)	**1.9106**	1.5535
SNOW 4	2.0149	0.4881	1.3189	0.8725	0.6501	1.3614	0.3303	(0.2585)	**2.0865**	2.0985
SNOW 5	1.9177	0.4606	1.2745	1.0776	0.5498	1.1969	0.3618	(0.2066)	**2.3013**	2.1352

DISCUSSION

From the above experiments, we can conclude that for some haze contexts, such as the last two images of Fig. 4, where the state-of-the-art methods perform well, they seem more natural than our proposed method. Despite its good performance at haze removal and enhancement of global quality of complicated image contexts, there is still room to improve the behavior of our proposed method by considering amplified noise and the boundary artifacts between dark and bright regions in the resulting image, which would be relieved through a good labeling of pixels.

The main difficulty with our method is that it is not completely automatic. Through the interactive graph cut based segmentation,[31,32] the user may need to relabel the pixels that are not well identified from a first segmentation until all pixels in the image get the right labeling.

One may ask how we can determine or know whether the selected bright area (sky or snow, for instance) is

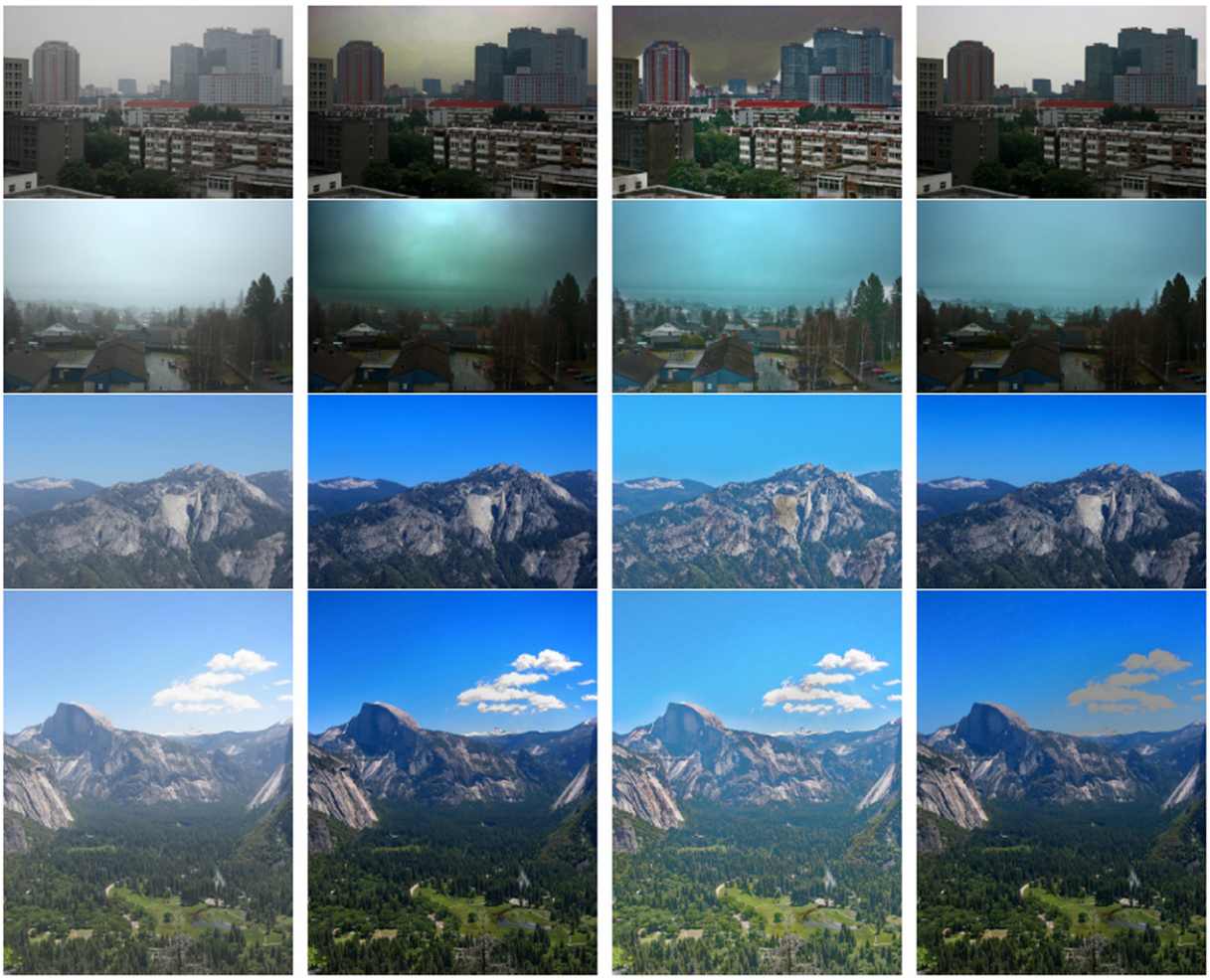

(a) (b) (c) (d)

Figure 4. From top to bottom, the images correspond to SKY 1, SKY 2, SKY 3 and SKY 4, respectively. (a) Original image, (b) He's method (DCP), (c) Tarel's method, (d) our method.

Table II. The scores of the *FADE*, *CNC* and *CS* metrics corresponding to the images dehazed by He's method, Tarel's method and our method and presented in Fig. 4. The best scores of *FADE*, *CNC* and *CS* are given in brackets, bold and underlined, respectively. A good reconstruction is denoted by *FADE* scores close to zero and high scores of *CNC* and *CS*.

	Original image	He's method			Tarel's method			Our method		
	FADE	*FADE*	*CNC*	*CS*	*FADE*	*CNC*	*CS*	*FADE*	*CNC*	*CS*
SKY 1	1.0172	0.5244	1.5756	0.6867	0.4230	1.5489	0.5499	(0.2837)	**1.8376**	0.8036
SKY 2	2.5307	0.6273	1.7948	1.0534	0.6286	1.7709	0.5288	(0.4293)	**1.9776**	1.1396
SKY 3	1.1784	0.4303	**2.0221**	0.8833	0.4631	1.9996	0.4685	(0.2572)	1.9267	0.9075
SKY 4	0.9123	0.3222	**2.0118**	1.0406	0.4282	1.9831	0.3126	(0.2061)	1.9504	1.0681

large enough or well segmented. For the sake of simplicity, we assume that it is possible for the user to change the segmentation that has been made if the output looks saturated or to assume that the whole image is bright. As we have said previously, it is possible to reduce chromatic distortions in the sky and similar regions using a dehazing algorithm like DCP by increasing the patch size. However, at the same time, in a scenario in which all regions in the scene except the sky region are dark, the output image looks almost the same as its corresponding hazy input image. Therefore, in that specific case, the multiscale of Ref. 11 may not be sufficient to solve the saturation issue or remove the fog.

One important point here is that the haze prior may change according to the context in which the haze occurs. Therefore, it is hard to introduce a single framework or single prior that works in any context. Moreover, in a heavy haze, it is always a good idea to improve the visibility of the foreground, since enhancement of the far region may

suppose that the data are available in the input image. However, this assumption is not valid in the case of a heavy haze. Many scenarios are then possible in that kind of application, and the priors that will be applied for some specific applications may fail in other cases.

CONCLUSION

We have proposed an approach that combines a local contrast enhancement method with the most popular and widely used dehazing method, DCP. Since the latter fails for images containing large bright regions such as sky and snow, we proceeded by segmenting the image into two parts, namely, bright and dark. To meet its prior hypothesis, DCP was only applied on the dark part. We applied BCP, which is an adjusted contrapositive form of the DCP through the STRESS approach, on the bright part. The resulting dehazed images outperform the results of the DCP for complicated contexts of hazy images showing snow and sky scenes in terms of the perceived quality. Future work may consider automatic segmentation and optimal separation between areas, which will be tested on a large image dataset.

REFERENCES

[1] L. Crewe and R. R. Brooks, "Atmospheric attenuation reduction through multi-sensor fusion," Proc. SPIE **3376**, 102–109 (1998).

[2] N. S. Kopeika, *A System Engineering Approach to Imaging* (SPIE Press, Bellingham, 1998).

[3] J. P. Oakley and B. L. Satherley, "Improving image quality in poor visibility conditions using a physical model for contrast degradation," IEEE Trans. Image Process. **7**, 167–179 (1998).

[4] S. G. Narasimhan and S. K. Nayar, "Chromatic framework for vision in bad weather," *Proc. IEEE Conf. Computer Vision and Pattern Recognition, 2000* (IEEE, Piscataway, NJ, 2000), Vol. 1, pp. 598–605.

[5] Y. Y. Schechner, S. G. Narasimhan, and S. K. Nayar, "Instant dehazing of images using polarization," *Proc. 2001 IEEE Computer Society Conf. Computer Vision and Pattern Recognition, 2001* (IEEE, Piscataway, NJ, 2001), Vol. 1, pp. 1–325.

[6] T. Wiesemann and X. Jiang, "Fog augmentation of road images for performance analysis of traffic sign detection algorithms," *Int'l. Conf. Advanced Concepts for Intelligent Vision Systems* (Springer, 2016), pp. 685–697.

[7] S. Q. Duntley, "The reduction of apparent contrast by the atmosphere," JOSA **38**, 179–191 (1948).

[8] H. Koschmieder, *Theorie der Horizontalen Sichtweite: Kontrast und Sichtweite* (Keim & Nemnich, 1925).

[9] V. Whannou de Dravo and J. Y. Hardeberg, "STRESS for dehazing," *In Colour and Visual Computing Symposium (CVCS)* (IEEE, Piscatway, NJ, 2015), pp. 1–6.

[10] J. El Khoury. Model and quality assessment of single image dehazing http://www.theses.fr/s98153, 2016.

[11] K. He, J. Sun, and X. Tang, "Single image haze removal using dark channel prior," IEEE Trans. Pattern Anal. Mach. Intell. **33**, 2341–2353 (2011).

[12] K. Tang, Y. Yang, and J. Wang, "Investigating haze-relevant features in a learning framework for image dehazing," *IEEE Conf. Computer Vision and Pattern Recognition (CVPR)* (IEEE, Piscataway, NJ, 2014).

[13] V. Whannou de Dravo, "*Dehazing with STRESS*", Master's thesis (Gjøvik University College, Norway, 2015).

[14] J. Kopf, B. Neubert, B. Chen, M. Cohen, D. Cohen-Or, O. Deussen, M. Uyttendaele, and D. Lischinski, "Deep photo: Model-based photograph enhancement and viewing," ACM Trans. Graph. **27**, 116:1–116:10 (2008).

[15] L. Schaul, C. Fredembach, and S. Süsstrunk, "Color image dehazing using the near-infrared," *Proc. IEEE Int'l. Conf. Image Processing (ICIP)* (IEEE, Piscataway, NJ, 2009), LCAV-CONF-2009-026.

[16] C. Feng, S. Zhuo, X. Zhang, L. Shen, and S. Susstrunk, "Near-infrared guided color image dehazing," *20th IEEE Int'l. Conf. on Image Processing (ICIP) 2013* (IEEE, Piscataway, NJ, 2013), pp. 2363–2367.

[17] R. Fattal, "Single image dehazing," ACM Trans. Graph. **27**, 72:1–72:9 (2008).

[18] J.-P. Tarel and N. Hautière, "Fast visibility restoration from a single color or gray level image," *Proc. IEEE Int'l. Conf. Computer Vision (ICCV'09)* (IEEE, Piscataway, NJ, 2009), pp. 2201–2208, http://perso.lcpc.fr/tarel.jean-philippe/publis/iccv09.html.

[19] R. T. Tan, "Visibility in bad weather from a single image," *IEEE Conf. Computer Vision and Pattern Recognition, 2008. CVPR 2008* (IEEE, Piscataway, NJ, 2008), pp. 1–8.

[20] A. Galdran, J. Vazquez-Corral, D. Pardo, and M. Bertalmo, "A variational framework for single image dehazing," in *Computer Vision—ECCV 2014 Workshops*, edited by Lourdes Agapito, Michael M. Bronstein, and Carsten Rother, Lecture Notes in Computer Science (Springer, 2015), Vol. 8927, pp. 259–270.

[21] A. Galdran, J. Vazquez-Corral, D. Pardo, and M. Bertalmio, "Enhanced variational image dehazing," SIAM J. Imaging Sci. **8**, 1519–1546 (2015).

[22] V. J. Whannou de Dravo and J. Y. Hardeberg, "Multiscale approach for dehazing using the STRESS framework," J. Imaging Sci. Technol. **60**, 010409 (2016).

[23] Ø. Kolås, I. Farup, and A. Rizzi, "Spatio-temporal retinex inspired envelope with stochastic sampling: a framework for spatial color algorithms," J. Imaging Sci. Technol. **55**, 040503 (2011).

[24] A. Rizzi, C. Gatta, and D. Marini, "A new algorithm for unsupervised global and local color correction," Pattern Recognit. Lett. **24**, 1663–1677 (2003).

[25] S. Shwartz, E. Namer, and Y. Y. Schechner, "Blind haze separation," *IEEE Computer Society Conf. Computer Vision and Pattern Recognition* (IEEE, Piscataway, NJ, 2006), Vol. 2, pp. 1984–1991.

[26] N. Hautière, J.-P. Tarel, D. Aubert, and E. Dumont, "Blind contrast enhancement assessment by gradient ratioing at visible edges," Image Analysis & Stereology J. **27**, 87–95 (2008).

[27] L. K. Choi, J. You, and A. C. Bovik, "Referenceless prediction of perceptual fog density and perceptual image defogging," IEEE Trans. Image Process. **24**, 3888–3901 (2015).

[28] S. Fang, J. Yang, J. Zhan, H. Yuan, and R. Rao, "Image quality assessment on image haze removal," *Control and Decision Conf. (CCDC), 2011 in Chinese* (IEEE, Piscataway, NJ, 2011), pp. 610–614.

[29] F. Guo, J. Tang, and Z.-X. Cai, "Objective measurement for image defogging algorithms," J. Central South University **21**, 272–286 (2014).

[30] H. Lu, Y. Li, S. Nakashima, and S. Serikawa, "Single image dehazing through improved atmospheric light estimation," Multimedia Tools and Appl. **75**, 17081–17096 (2016).

[31] C. Rother, V. Kolmogorov, and A. Blake, "GrabCut: Interactive foreground extraction using interated graph cuts," *SIGGRAPH* (ACM, New York, NY, 2004), pp. 309–314.

[32] B. Klava and N. S. T. Hirata, Segmentlt—interactive image segmentation tool, http://segmentit.sourceforge.net. Accessed: 2017-02-24.